

IEEE ICME 2024 GRAND CHALLENGE: LOW-POWER EFFICIENT AND ACCURATE FACIAL-LANDMARK DETECTION FOR EMBEDDED SYSTEMS

Zong-Wei Hong, Yu-Chen Lin

ABSTRACT

The domain of computer vision has experienced significant advancements in facial-landmark detection, becoming increasingly essential across various applications such as augmented reality, facial recognition, and emotion analysis. Unlike object detection or semantic segmentation, which focus on identifying objects and outlining boundaries, facial-landmark detection aims to precisely locate and track critical facial features.

However, deploying deep learning-based facial-landmark detection models on embedded systems with limited computational resources poses challenges due to the complexity of facial features, especially in dynamic settings. Additionally, ensuring robustness across diverse ethnicities and expressions presents further obstacles. Existing datasets often lack comprehensive representation of facial nuances, particularly within populations like those in Taiwan.

This paper introduces a novel approach to address these challenges through the development of a knowledge distillation method. By transferring knowledge from larger models to smaller ones, we aim to create lightweight yet powerful deep learning models tailored specifically for facial-landmark detection tasks. Our goal is to design models capable of accurately locating facial landmarks under varying conditions, including diverse expressions, orientations, and lighting environments. The ultimate objective is to achieve high accuracy and real-time performance suitable for deployment on embedded systems. This method was successfully implemented and achieved a top 6th place finish out of 165 participants in the IEEE ICME 2024 PAIR competition.

Index Terms— Facial landmark detection, Deep learning, Low power

1. INTRODUCTION

To improve the accuracy of facial landmark detection using a *single model*, we employ a two-step approach, dividing the process into face detection and landmark detection. Specifically, we utilize on-the-fly packages such as OpenCV [1] or dlib [2] due to time constraints in pre-processing. It is important to note that **NEITHER** of these packages is based on deep learning techniques. Another advantage of this two-step approach is that it allows for potential enhancements in accu-

racy by substituting the face detector with potentially more powerful alternatives in the future.

In our approach, we employ the knowledge distillation technique to enhance the performance of our models. Initially, we trained a Swin Transformer (SwinV2 [3]) utilizing the STAR Loss [4] function as our teacher model, yielding a promising score of 18.08 in the initial round of experimentation. Subsequently, leveraging the distilled knowledge from SwinV2, we employed it to train a more lightweight model, the MobileViT-v2 [5]. Remarkably, even in its nascent stage, the MobileViT-v2 showcased significant promise by achieving a score of 15.75 in the initial round of evaluation.

We will provide further details in the following section.

2. IMPLEMENTATION TECHNIQUES

2.1. Preliminary

Given a cropped face image \mathcal{I} , the main goal of facial landmark detection is to identify and recover the N facial landmarks, denoted as $\mathcal{P} = \{P_i = \{x_i, y_i\} | i = 1, \dots, N\}$. This task typically involves two distinct approaches that complement each other: regression-based and heatmap-based methods.

Due to their superior accuracy, we have opted to incorporate heatmap-based methods into the development of our approach. Specifically, for every landmark, we produce a corresponding heatmap. These normalized heatmaps can be understood as probability distributions representing the predicted facial landmarks. The predicted coordinates are extrapolated from the heatmaps utilizing a soft-Argmax [6] decoding technique.

Specifically, given a discrete probability distribution h , we assign the value h_k to represent the probability of the predicted landmark being positioned at $o_k \in \mathbb{R}^2$ for each predicted landmark \hat{P}_i . This calculation can be performed using the following formula.

$$\hat{P}_i = \sum_k h_k o_k \quad (1)$$

Therefore, we can employ the regression loss \mathcal{L}_{reg} to direct the training of our model. To maintain generality, we opt for the STAR loss [4] in our experimental setup.

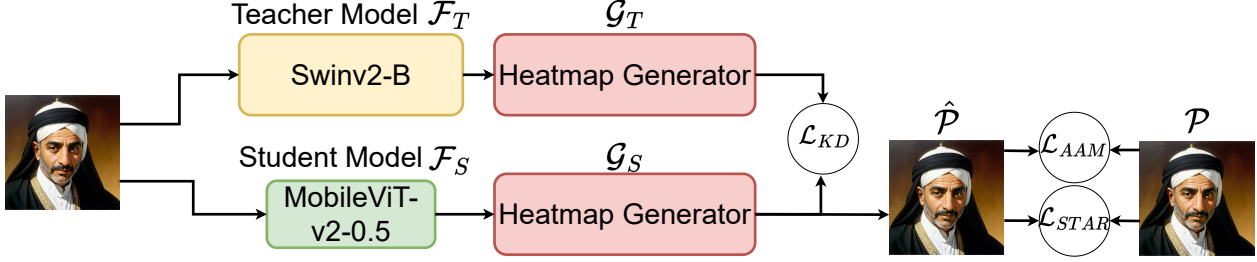


Fig. 1. We propose a two-stage training process for our method. In the first stage, we train the teacher model, denoted as \mathcal{F}_T , using a combination of two loss functions: \mathcal{L}_{AAM} and \mathcal{L}_{STAR} . Subsequently, in the second stage, we train the student model by introducing an additional loss function, \mathcal{L}_{KD} .

2.2. Model Architecture

There are primary two components of our model: the feature extractor backbone, denoted as $\mathcal{F} : \mathbb{R}^{3 \times 256 \times 256} \rightarrow \mathbb{R}^{C \times 64 \times 64}$, and the heatmap generator, represented by $\mathcal{G} : \mathbb{R}^{C \times 64 \times 64} \rightarrow \mathbb{R}^{N \times 64 \times 64}$, which are illustrated in Figure 1. Therefore, we can define the predicting process as follows:

$$\hat{P}_i = \sum_k [\mathcal{G}(\mathcal{F}(\mathcal{I}))]_k^i o_k, \quad (2)$$

where $[\mathcal{G}(\mathcal{F}(\cdot))]_k^i$ represents the predicted probability heatmap for the i -th facial landmark at location o_k . It is noteworthy that, for the purpose of enhancing the heatmap's precision, we have integrated the Anisotropic Attention Module (AAM), as detailed in [7]. The AAM functions as an attention module, tasked with generating a point-edge heatmap that functions as an attention mask. This module ensures that the heatmap demonstrates qualities akin to a blend of Gaussian distribution and neighboring boundary distribution. During the training phase, we employ \mathcal{L}_{AAM} to guide the edge and point, and we highly encourage readers to refer to the original paper [7] for comprehensive details.

Recently, it has become evident that transformer-based architectures outperform CNNs. Moreover, given that this challenge expected a low-power, efficient solution for embedded systems, architecture specifically designed for mobile devices such as MobileViT is definitely a good choice. Consequently, this paper adopts the transformer-based architecture as the cornerstone of our features, employing knowledge distillation to refine our approach.

2.2.1. Teacher architecture

For the selection of our teacher model, we have chosen SwinV2-B [3], pre-trained on ImageNet-1K. In our implementation, we have omitted the classifier layer, utilizing only the feature extractor component as the backbone for our teacher model. To ensure compatibility with the input dimensions of the heatmap generator \mathcal{G} , we have incorporated an upsample layer to the output of SwinV2.

2.2.2. Student architecture

For our student model selection, we've opted for MobileViT-v2-0.5 [5] as our backbone due to its suitability for our embedding requirements. We've specifically chosen to exclude the classifier layer, utilizing solely the feature extractor component as the backbone, and subsequently increasing the feature dimension to 64 through upsampling. However, in comparison to the original version, we have made partial structural revisions to ensure its compatibility with tflite-runtime versions up to 2.11.0.

The specific revision involves replacing the "fold" and "unfold" operations in PyTorch with "reshape" and "permute". However, the "permute" operation does not support 6 dimensions for tflite-runtime versions up to 2.11.0. Therefore, we split the original 6-dimensional input into multiple 5-dimensional tensors, permute each 5-dimensional tensor, and finally concatenate them back into a 6-dimensional tensor. Below is our code (partly pseudo):

```
# mobilevit_block.py
def unfolding_pytorch(...):
    ...
    #Original code
    #patches = nn.functional.unfold(
    #    ...
    #)
    feature_map = feature_map.reshape(...)
    x_splits = torch.split(...)
    splited_transposed_tensors = []
    for x_split in x_splits:
        squeezed_tensor = torch.squeeze(x_split,
            dim=-1)
        splited_transposed_tensors.append(
            torch.unsqueeze(
                squeezed_tensor.permute(0, 1, 3, 2, 4),
                dim=3)
        )
    feature_map = torch.cat(
        splited_transposed_tensors,
        dim=3)
    )
def folding_pytorch(...)
    #Original code
    #feature_map = nn.functional.fold(
```

```

# ...
#)
.....
# Similar strategy here.
return feature_map

```

2.2.3. Heatmap generator architecture

Our heatmap generator architecture, as outlined by [7], employs Convolution2D layers with sigmoid activation for edge and point prediction, alongside Convolution2D layers with instance normalization and ReLU activation for heatmap prediction.

2.3. Knowledge Distillation Loss

For training teacher model, we only use \mathcal{L}_{reg} and \mathcal{L}_{AAM} for supervising. However, in order to facilitate the learning process for the lightweight model, we have designed the strainforward loss \mathcal{L}_{KD} to efficiently transfer primary features from the teacher model to the student model, defined as:

$$\mathcal{L}_{KD} = \sum_{i=1}^N \sum_k ||[\mathcal{G}_T(\mathcal{F}_T(\cdot))]_k^i - [\mathcal{G}_S(\mathcal{F}_S(\cdot))]_k^i||_2, \quad (3)$$

where \mathcal{F}_T denotes the teacher feature extractor, \mathcal{F}_S denotes the student feature extractor, \mathcal{G}_T denotes the teacher heatmap generator and \mathcal{G}_S denotes the student heatmap generator.

3. EXPERIMENT

3.1. Experiment setting

All experiments are conducted using the RTX 3090 and Intel i7-12700K configurations.

The data augmentation process employed in [4, 7] remains consistent across all experiments. It involves generating the input image through two sequential steps: (1) Cropping the facial regions and resizing them to 256x256 dimensions. (2) Implementing augmentations including random rotation (45°), random scaling ($\pm 10\%$), random crop ($\pm 18\%$), random blur (40%), random gray (20%), random occlusion (40%), and random horizontal flip (50%)

For the training strategy, we have designated a learning rate of $2e-4$ for the backbone component and $1e-3$ for the heatmap component during both teacher and student training, utilizing the AdamW [8] optimizer. The batch size for training both the teacher and student is configured to be 16.

For the dataset, we partitioned the training dataset into a training set and a validation set using a 10:1 ratio and selected the model with the lowest normalized mean error (NME).

Method	GFlops	MMACs	Params (M)	Inference Time (ms)	Val NME (%)
Hourglasses	10.4436	5190.2	1.8747	88	3.78
mobileFormer-26m	0.288	142.478	1.5152	31.1	5.31
MobileViT-v2-0.5 w/o \mathcal{L}_{KD}	1.1865	581.354	1.1419	23.8	5.13
MobileViT-v2-0.5 (Ours)	1.1865	581.354	1.1419	23.8	4.96

Table 1. Experimental Comparison on the validation dataset.

Method	Complexity	Model Size	Speed	Power	Accuracy
MobileViT-v2-0.5 (Ours-fp16)	1162.7	2.64258	609518.7	2251.18	15.27

Table 2. Experimental Comparison on the host machine.

3.2. Model Complexity & Model Execution Efficiency

The model complexity is detailed in table 1. In order to validate our proposed framework, we conducted tests using another transformer-based model (mobileFormer-26m) and CNNs (Hourglasses). While the mobileFormer-26m appeared to be the most promising solution, we opted not to submit it as it failed to convert into tflite under $tflite\text{-runtime} < 2.11.0$.

Layer	Output size	Repeat	Output channels
Image	256×256	-	-
Conv- $3 \times 3, \downarrow 2$	-	1	32α
MV2	128×128	1	64α
MV2, $\downarrow 2$	-	1	128α
MV2	64×64	2	128α
MV2, $\downarrow 2$	-	1	256α
MobileViTv2 block	32×32	1	$256 * \alpha (d = 128\alpha)$
MV2, $\downarrow 2$	-	1	384α
MobileViTv2 block	16×16	1	$384\alpha (d = 192\alpha)$
MV2, $\downarrow 2$	-	1	512α
MobileViTv2 block	8×8	1	$512\alpha (d = 256\alpha)$
UpSample	64×64	1	$512\alpha (d = 256\alpha)$
Conv-Sigmoid	64×64	1	51
Conv-Sigmoid	64×64	1	8
E2P Transform	64×64	1	51
Elementwise dot	64×64	1	51
Conv-Relu	64×64	1	51
Elementwise dot	64×64	1	51
Soft Argmax	64×64	1	51
Conv	64×64	1	51
Conv	64×64	1	51
Conv	64×64	1	51
Elementwise sum	64×64	1	51

Table 3. The student model architecture. We utilize a scaling factor of $\alpha = 0.5$ within our methodology.

3.3. Normalized Mean Square Error

To evaluate the proposed method, we conduct experiments on the validation set. Our observations suggest a trend wherein an increase in parameter count leads to improved performance. This phenomenon is also corroborated in [9].

3.4. Converted Model Complexity and Execution Efficiency

The model information after conversion is displayed in table 2. It should be noted that on the D9300 platform, certain operations may not be compatible with NNAPI, potentially allowing for further enhancements in speed and power efficiency.

3.5. Model Structure

We provide the student model architecture in Table 3

4. CONCLUSION

In this paper, we present a pioneering framework solution for embedding systems. Specifically, we leverage the knowledge distillation loss to steer the lightweight model, resulting in superior performance. Our approach not only enhances efficiency but also maintains high accuracy, thus promising significant advancements in embedding system design.

5. REFERENCES

- [1] G. Bradski, “The OpenCV Library,” *Dr. Dobbs’s Journal of Software Tools*, 2000.
- [2] Vahid Kazemi and Josephine Sullivan, “One millisecond face alignment with an ensemble of regression trees,” in *2014 IEEE Conference on Computer Vision and Pattern Recognition*, 2014, pp. 1867–1874.
- [3] Ze Liu, Han Hu, Yutong Lin, Zhuliang Yao, Zhenda Xie, Yixuan Wei, Jia Ning, Yue Cao, Zheng Zhang, Li Dong, et al., “Swin transformer v2: Scaling up capacity and resolution,” in *Proceedings of the IEEE/CVF conference on computer vision and pattern recognition*, 2022, pp. 12009–12019.
- [4] Zhenglin Zhou, Huaxia Li, Hong Liu, Nanyang Wang, Gang Yu, and Rongrong Ji, “Star loss: Reducing semantic ambiguity in facial landmark detection,” in *Proceedings of the IEEE/CVF Conference on Computer Vision and Pattern Recognition*, 2023, pp. 15475–15484.
- [5] Sachin Mehta and Mohammad Rastegari, “Separable self-attention for mobile vision transformers,” *arXiv preprint arXiv:2206.02680*, 2022.
- [6] Aiden Nibali, Zhen He, Stuart Morgan, and Luke Prendergast, “Numerical coordinate regression with convolutional neural networks,” *arXiv preprint arXiv:1801.07372*, 2018.
- [7] Yangyu Huang, Hao Yang, Chong Li, Jongyoo Kim, and Fangyun Wei, “Adnet: Leveraging error-bias towards normal direction in face alignment,” in *Proceedings of the IEEE/CVF International Conference on Computer Vision*, 2021, pp. 3080–3090.
- [8] Ilya Loshchilov and Frank Hutter, “Decoupled weight decay regularization,” *arXiv preprint arXiv:1711.05101*, 2017.
- [9] Ali Pourramezan Fard and Mohammad H Mahoor, “Facial landmark points detection using knowledge distillation-based neural networks,” *Computer Vision and Image Understanding*, vol. 215, pp. 103316, 2022.